PRAMANA
— journal of
physics

Vol. 75, No. 4
October 2010
pp. 691–708

Comparative study of runaway electron diffusion in the rise phase of low q_a and normal q_a discharges in the SINP tokamak

RAMESH NARAYANAN[1,2,*] and A N SEKAR IYENGAR[1]
[1]Saha Institute of Nuclear Physics, I/AF, Bidhan Nagar, Kolkata 700 064, India
[2]Present address: Centre for Energy Studies, Indian Institute of Technology, Delhi, Hauz Khas, New Delhi 110 016, India
[*]Corresponding author. E-mail: rams75apr@yahoo.co.in

MS received 28 July 2009; revised 4 May 2010; accepted 14 May 2010

Abstract. The behaviour of runaway electrons in the SINP tokamak, which can be operated in a normal edge safety factor (q_a) (NQ) discharge configuration as well as in a low q_a (LQ) configuration, was experimentally investigated, during the initial plasma generation phase. An energy analysis of the runaway electron dynamics in the rise phase of the SINP tokamak discharges was also made. A comparison of the runaway electron diffusion coefficients in NQ and LQ is carried out in this paper.

Keywords. Runaway electrons; tokamak; edge safety factor; diffusion coefficient; confinement.

PACS Nos 52.25.Xz; 52.70.La; 52.55.Fa; 52.38.Ph; 82.80.Ej

1. Introduction

The behaviour of runaway electron has been studied in great detail in a number of tokamaks and RFPs. In tokamaks, the accelerating force is primarily the toroidal electric field (E_T) which produces and sustains the plasma current. When the toroidal electric field is greater than the critical electric field (dependent on density, temperature and effective charge) [1], electrons in the tail of the velocity distributions can be accelerated to relativistic velocities and these are termed runaway electrons. Confinement of these high-energy electrons for a long time in the tokamak can cause serious damage to the vessel walls and surrounding structures, especially in disruptive discharges [2–4]. They are useful diagnostics for magnetic turbulence. Hence, there are efforts to study these electrons by various techniques and under various conditions [5–11].

The behaviour of runaway electrons was studied extensively in various tokamaks in the past few decades. In LT-3, runaway electrons were observed to be confined

in regions where $r/a \sim 0.4$, with runaway energies (W_{RE}) less than 300 keV and diffusion coefficients (D_{RE}) of about 1–50 m^2/s [12]. In LT-4 [13], hard X-ray studies were carried out in the current rise phase correlating them with the edge safety factor (q_a). Average energies ranging from a few keV to 200–500 keV were observed. Similar edge runaway generations were observed in the ISTTOK tokamak, gaining energies of about 6–35 keV before being lost and $D_{\mathrm{RE}} \sim 2$–$20\ \mathrm{m}^2/\mathrm{s}$ and ratio of runaway confinement times (τ_{RE}) to plasma confinement times (τ_{p}) ~ 1 [14]. In PLT tokamak [15,16], estimates from PLT limiter fluctuations gave D_{RE} was found to be $\sim$0.06–1 m^2/s for $W_{\mathrm{RE}} \sim 0.4$–1 MeV and $\sim$0.4–0.8 m^2/s for $W_{\mathrm{RE}} \sim 8$–23 MeV electrons. In L-mode regimes of ASDEX, D_{RE} was observed to be $\sim 0.07\ \mathrm{m}^2/\mathrm{s}$ for 1 MeV electrons [17]. In more recent machines, with much better confinement properties, runaways were observed to be generated and confined more towards the core and have much reduced diffusion coefficients (e.g. JET: $D_{\mathrm{RE}} \sim 0.2\ \mathrm{m}^2/\mathrm{s}$ for $r/a < 0.5$ [18]; TEXTOR: $D_{\mathrm{RE}} < 0.01\ \mathrm{m}^2/\mathrm{s}$ for 25 MeV [19]; Tore Supra: $D_{\mathrm{RE}} = 0.1$–$0.2\ \mathrm{m}^2/\mathrm{s}$ in the range 100–200 keV [20]; FTU: $\sim 0.03\ \mathrm{m}^2/\mathrm{s}$ at current flat top [21]). Most of the parallel current densities at the edge of the reversed-field pinch devices were observed to be carried by the nonthermal electron distribution, and found to have significant effects on the edge physics [22] (for e.g., ZT-40M: superthermal electron energies $W_{\mathrm{RE}} \sim 0.6$–6 keV and energy flux $q_{||} \sim 140\ \mathrm{MW}/\mathrm{m}^2$ [23], TPE-1RM20: $W_{\mathrm{RE}} \sim 2$–8 keV [24]; RFX: $T_\perp \sim T_{||} \approx 100$–200 eV and energy flux $q_\perp \sim 100\ \mathrm{MW}/\mathrm{m}^2$ [25]).

The SINP tokamak has the unique characteristic of being able to operate in normal edge safety factor, q_a (NQ) ($q_a > 2$) and low q_a (LQ) ($0 < q_a < 2$) [26], wherein $q_a = aB_{\mathrm{T}}/RB_{\mathrm{p}}$ for a circular cross-sectional plasma, with R being the major radius in metre and a the minor radius of the toroidal chamber in metre. B_{T} and $B_{\mathrm{p}}(=\mu_0 I_{\mathrm{p}}/2\pi a)$ are the applied toroidal and poloidal magnetic fields (in tesla). I_{p} is the total plasma current in kA. The LQ regime [27–29] can be further classified as very low q_a (VLQ) ($1 < q_a < 2$) [30–32] and ultra-low q_a (ULQ) ($0 < q_a < 1$) [33–36] regions. As $q_a = aB_{\mathrm{T}}/RB_{\mathrm{p}}$, different q_a discharges can be obtained by varying a, B_{T} and the externally applied toroidal electric field (E_{T}), which will have a control on the plasma current I_{p}. E_{T} can be expressed in terms of the applied Joule heating voltage (V_{JH}), as $E_{\mathrm{T}} = V_{\mathrm{JH}}/2N_{\mathrm{Tr}}\pi R$. N_{Tr} is the ratio of the primary to the secondary transformer winding of the Joule heating mechanism in a tokamak, with the toroidal chamber being the one-turn secondary of the transformer. $N_{\mathrm{Tr}} = 52$ for SINP tokamak.

Preliminary studies regarding the runaway characteristics during the start-up phase of VLQ discharges, in the SINP tokamak [26], presents an alternative method to mitigate the runaway electrons by controlling the B_{T}. The VLQ regime was attained by decreasing B_{T} and it was found that not only did hard X-ray intensity decrease as q_a values decreased but also the point of the start of the emission ($t_{\mathrm{HX}}^{\mathrm{beg}}$) was observed to be ahead in time. It was pointed out that eliminating these electrons at an early phase also helped in the evolution of the rest of the discharge. However, an estimate of the runaway energy dependence was not possible in that work due to limitations in the diagnostics. Presently we have a spectroscopic amplifier and MCA, allowing for the energy calibration of the emitted bremsstrahlung. It was also experimentally found that if the time taken to cross $q_a + 1$ was less than the resistive diffusion time (τ_{R}), then the discharges were observed to enter

q_a. Thereafter the main factor of generating relatively more stable ULQ discharges in the SINP tokamak has been realized by increasing the rate of rise of current [29]. From this viewpoint, an energy analysis of the hard X-ray bursts was carried out by varying E_{T}, which has a direct impact on the plasma current and thereby the energy of the system. Hence, we proceed to check the dependence of runaway energy in the NQ and LQ regimes. A comparison of the behaviour of these highly energetic electrons, in LQ and NQ discharges, have been put forth.

Section 2 presents the experimental set-up which includes a description of the SINP tokamak and the diagnostics. In §3, we depict the experimental observations as well as the average runaway characteristics during the parametric scan. In §4 we numerically estimate, using experimental data, the runaway diffusion coefficients (D_{RE}) as well as its confinement time (τ_{RE}). Section 5 discusses the results of the work presented in this paper.

2. Experimental set-up

2.1 *SINP Tokamak*

The SINP Tokamak (Saha Institute of Nuclear Physics tokamak) is a small iron core machine having a circular cross-section. It has a major radius of 0.3 m and a minor radius of 0.075 m. Discharges, produced through the Joule heating (JH) mechanism, can operate in the range of a few kA peak current to a maximum of 75 kA with pulse durations varying from 2 to 5 ms. The toroidal magnetic field (B_{T}) for the present experiments has been varied from 0.2 to 1.3 T. The SINP tokamak has a pair of movable limiters which can be used to vary the minor radius from 0.045 to 0.075 m.

The equilibrium is provided by an aluminium conducting shell of 0.007 m thickness outside the stainless steel vacuum chamber in addition to a set of magnetic coils which produces the vertical magnetic field.

2.2 *Diagnostics*

We used mainly the poloidal flux loop coil to measure the loop voltage (V_{loop}), Rogowskii coil for the discharge current (I_{p}) and the hard X-ray monitor for the present experiments.

The limiter bremsstrahlung monitor was a $3'' \times 3''$ NaI(Tl) detector, with its line of sight intersecting the plane containing the SINP tokamak fixed limiter 1 [37]. The detector, shielded by Mu metal, was placed 2 m away from the chamber, so as to minimize pickups from the large magnetic fields associated with tokamak discharges. The detectors was calibrated mostly using standard sources [^{22}Na (511 keV and 1275 keV) and ^{60}Co (1173.2 KeV and 1332.5 keV) and ^{133}Ba (81 keV and 356 keV)]. The ^{133}Ba source was only available for calibration of the detectors during one of the earlier experimental sessions. The conditions of the detector set-up was kept constant in all the subsequent experiment sessions. The variations in the calibrations made using the other sources, were observed to be less than 5%. Hence, we considered the calibration factors obtained from ^{133}Ba source as the same

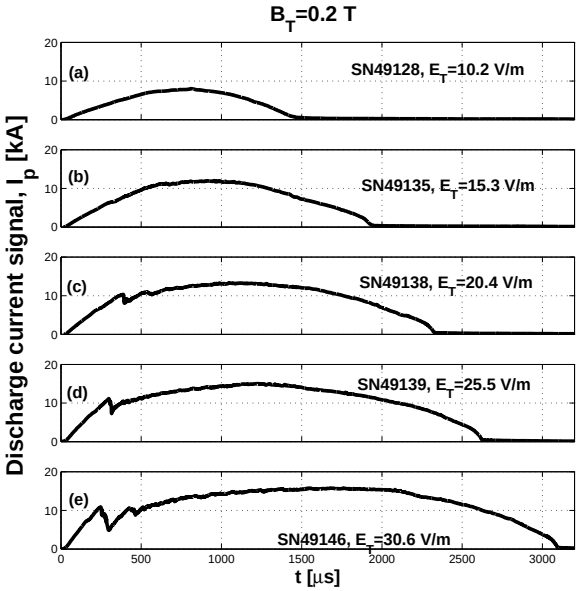

Figure 1. The depiction of the discharge current (I_p) evolution for five typical discharges, observed in the low-B_T discharge regime for the E_T scan: (**a**) $E_\mathrm{T} = 10.2$ V/m, (**b**) $E_\mathrm{T} = 15.3$ V/m, (**c**) $E_\mathrm{T} = 20.4$ V/m, (**d**) $E_\mathrm{T} = 25.5$ V/m and (**e**) $E_\mathrm{T} = 30.6$ V/m.

for all the remaining experimental sessions. The estimated fitted calibration factor obtained was then used to record hard X-ray bursts during the plasma discharges directly in terms of energy.

3. Experimental results

Though runaway electrons can be observed during the rise phase, sustainment phase and the decay phase of the plasma current, for this paper, we have concentrated only on the rise phase, because in many cases the early phase generation of the highly energetic electrons decides their behaviour in the other phases. The rise phase (rs) is defined as the region wherein the total plasma current (I_p) is initiated and increases towards its peak value in the discharge. This phase is considered upto the region where I_p is 90% of its peak value.

Figures 1 and 2 depict the evolution of the plasma current in the SINP tokamak for varying externally applied toroidal electric fields at two different sets of other externally applied parameters. In figure 1, $B_\mathrm{T} = 0.2$ T whereas in figure 2, $B_\mathrm{T} = 1.3$ T. In the latter discharge a higher toroidal magnetic field has been applied with respect to the former, and so we shall henceforth demarcate the two sets of discharges as the low-B_T and high-B_T discharges respectively. The movable limiter was behind the fixed limiter and so the minor radius of the plasma (a) is 0.075 m in both scans.

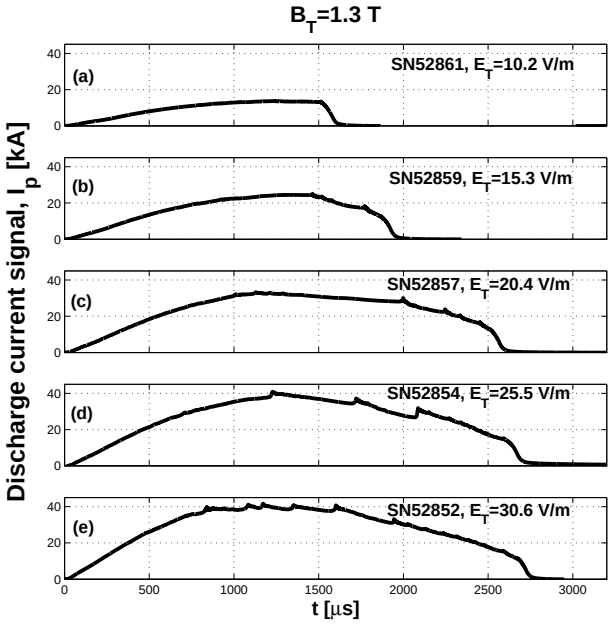

Figure 2. The depiction of the discharge current (I_p) evolution for five typical discharges, observed in the high-B_T discharge regime for the E_T scan: (**a**) $E_\mathrm{T} = 10.2$ V/m, (**b**) $E_\mathrm{T} = 15.3$ V/m, (**c**) $E_\mathrm{T} = 20.4$ V/m, (**d**) $E_\mathrm{T} = 25.5$ V/m and (**e**) $E_\mathrm{T} = 30.6$ V/m.

By increasing the applied E_T, one finds that the peak value of plasma current, I_p^pk, increases and so does the time of peaking. Figure 1 shows that for $E_\mathrm{T} = 10.2$ V/m, the current peaks at $\tau_\mathrm{pk} \sim 800$ μs with a peak value of $I_\mathrm{p}^\mathrm{pk} \sim 8$ kA, i.e., a rise time of $(\mathrm{d}I_\mathrm{p}/\mathrm{d}t) \approx 10$ MA/s. The peak value increases with E_T and attains a value of $I_\mathrm{p}^\mathrm{pk} \sim 16$ kA for $E_\mathrm{T} = 30.6$ V/m. Higher E_T discharges are also observed to have peak currents of the same order. The time for current to peak is also seen to shift to a later time with E_T. Thus, at $E_\mathrm{T} = 30.6$ V/m, we find that $\tau_\mathrm{pk} \sim 1600$ μs. For $E_\mathrm{T} > 30.6$ V/m, one observes the current to peak at earlier times. The total discharge duration ($\tau_\mathrm{disch}^\mathrm{dur}$) is also observed to increase from $\tau_\mathrm{disch}^\mathrm{dur} \sim 1500$ μs at $E_\mathrm{T} = 10.2$ V/m to $\tau_\mathrm{disch}^\mathrm{dur} \sim 3100$ μs at $E_\mathrm{T} = 30.6$ V/m. For $E_\mathrm{T} > 35.7$ V/m, the discharges have been observed to reduce in discharge duration with $\tau_\mathrm{disch}^\mathrm{dur} \sim 2100$ μs at $E_\mathrm{T} = 45.9$ V/m. Prominent current crashes are also seen in the initial rise phase for $E_\mathrm{T} \geq 20.4$ V/m, which are observed to be associated to positive loop voltage spikes. These positive loop voltage spikes are associated to the LQ discharges being able to cross disruptive $m = 1, n = 1$ and $m = 2$, $n = 1$ modes, and enter the LQ regime. These crashes are observed to become more severe with increasing E_T and in the subsequent recovery phase after the crash, the rate of current rise is observed to decrease.

In figure 2, the discharge current is observed to rise to 13.71 kA in 1233 μs for $E_\mathrm{T} = 10.2$ V/m, i.e., $(\mathrm{d}I_\mathrm{p}/\mathrm{d}t) \approx 11.12$ MA/s. With increasing E_T, one finds a faster current rise rate, with the peak current, at $E_\mathrm{T} = 30.6$ V/m, being about

40.13 kA in 1134 μs, i.e., $(\mathrm{d}I_\mathrm{p}/\mathrm{d}t) \approx 35.39$ MA/s. This is much more than in the previous scan of figure 1e ($\approx$22 MA/s before the current crash and $\approx$7 MA/s after the recovery from the current crash). In fact, $(\mathrm{d}I_\mathrm{p}/\mathrm{d}t) \approx 70$ MA/s at $E_\mathrm{T} = 45.9$ V/m in this high-B_T scan. The duration of the discharge increases from 1616 μs at $E_\mathrm{T} = 10.2$ V/m to 2750 μs at $E_\mathrm{T} = 30.6$ V/m (figure 2). The severe crashes in the rise phase are also found to be absent in this scan.

The loss of the high-energy electrons from the discharge, monitored using a $3'' \times 3''$ NaI(Tl) detector, for lower B_T scan is shown in figure 3 and that for the higher-B_T scan is shown in figure 4, in terms of energy units. The HX emission, in the rise phase, is seen to be more denser in the latter scan (figure 4) than in the former (figure 3).

The time at which the first runaway burst ($t_\mathrm{HX}^\mathrm{beg}$) is observed in the low-B_T discharges is plotted in figure 5a and that for the high-B_T discharges is presented in figure 5b. From figure 5a, we can see that $t_\mathrm{HX}^\mathrm{beg}$ is varying in the range of 390 μs to 225 μs while in figure 5b the variation is in the range of 160 μs to 240 μs.

Further, from a comparison of the peaks in the hard X-ray bursts, in the two set of different B_T discharges, an increase of 10 is observed (figures 3 and 4), with the average runaway energy flux over the set of repeatable discharges, varying by about 4–5 at lower E_T values to as high as 8 at higher E_T (figures 6 and 7). This confirms the earlier experiments carried out in the SINP tokamak [26], which observed the mitigation of runaway electrons as the discharges transit from an NQ to an LQ

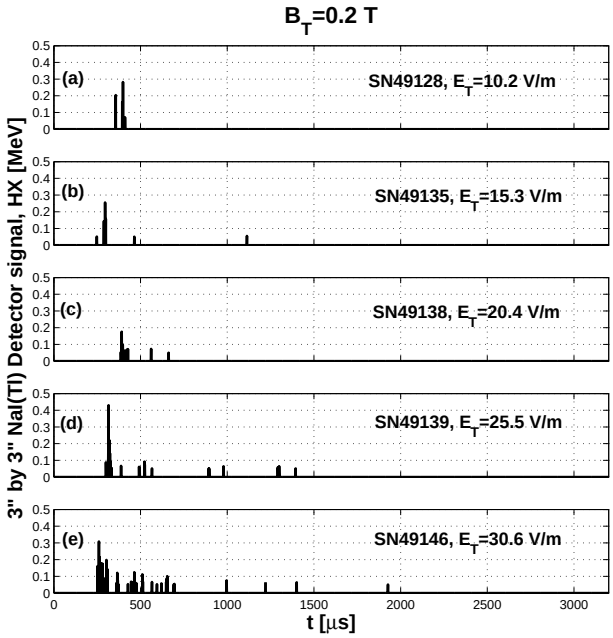

Figure 3. The depiction of the hard X-ray burst evolution, calibrated in terms of energy (HX), for five typical discharges, observed in the low-B_T discharge regime for the E_T scan: (**a**) $E_\mathrm{T} = 10.2$ V/m, (**b**) $E_\mathrm{T} = 15.3$ V/m, (**c**) $E_\mathrm{T} = 20.4$ V/m, (**d**) $E_\mathrm{T} = 25.5$ V/m and (**e**) $E_\mathrm{T} = 30.6$ V/m.

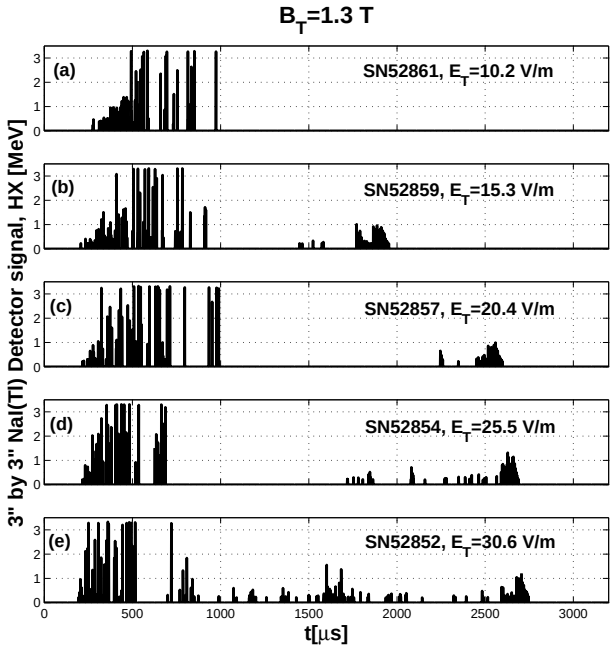

Figure 4. The depiction of the hard X-ray burst evolution, calibrated in terms of energy (HX), for five typical discharges, observed in the high-B_{T} discharge regime for the E_{T} scan: (**a**) $E_{\mathrm{T}} = 10.2$ V/m, (**b**) $E_{\mathrm{T}} = 15.3$ V/m, (**c**) $E_{\mathrm{T}} = 20.4$ V/m, (**d**) $E_{\mathrm{T}} = 25.5$ V/m and (**e**) $E_{\mathrm{T}} = 30.6$ V/m.

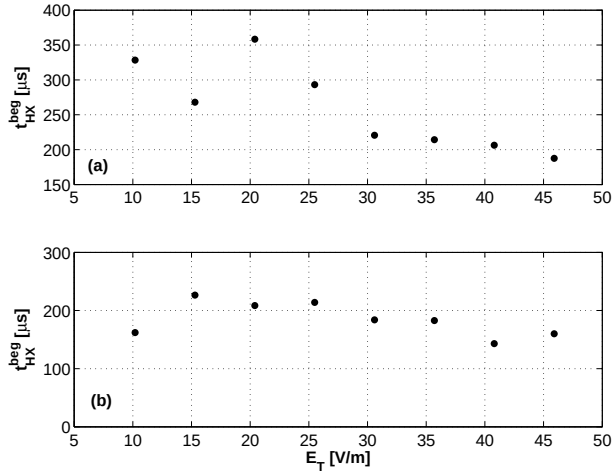

Figure 5. The variation with E_{T} of the time of first runaway burst from breakdown, $t_{\mathrm{HX}}^{\mathrm{beg}}$ in the rise phase; performed for discharges with (**a**) $B_{\mathrm{T}} = 0.2$ T, (**b**) $B_{\mathrm{T}} = 1.3$ T. Scatter in data over identical discharges is within the range of 50 μs.

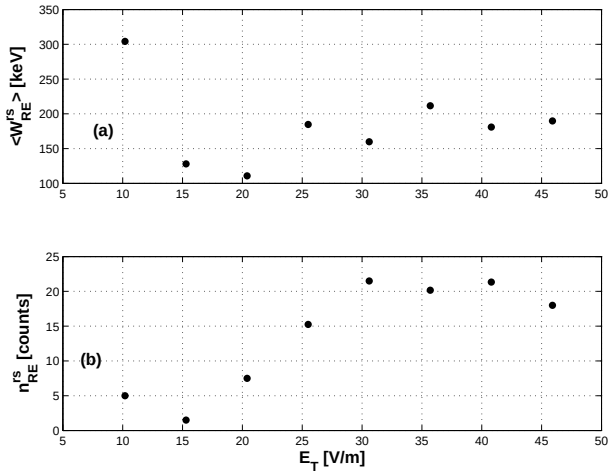

Figure 6. The runaway features in the rise phase of the E_{T} scan for discharges with $B_{\mathrm{T}} = 0.2$ T: (**a**) average limiter bremsstrahlung energy ($W^{\mathrm{rs}}_{\mathrm{RE}}$) in keV, (**b**) number of valid photons recorded ($n^{\mathrm{rs}}_{\mathrm{RE}}$). Scatter in data over identical discharges is within the range of 100 keV and 20 counts.

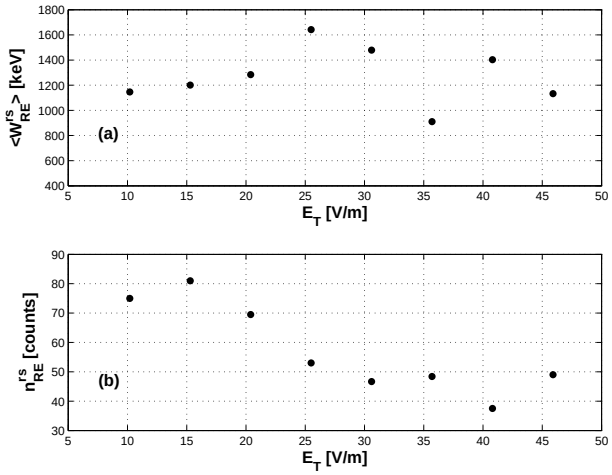

Figure 7. The runaway features in the rise phase of the E_{T} scan for discharges with $B_{\mathrm{T}} = 1.3$ T: (**a**) average limiter bremsstrahlung energy ($W^{\mathrm{rs}}_{\mathrm{RE}}$) in keV and (**b**) number of valid photons recorded ($n^{\mathrm{rs}}_{\mathrm{RE}}$). Scatter in data over identical discharges is usually within the range of 100 keV and 10 counts.

regime. An energy analysis of the transition was not possible in that paper. Here, we estimate the average energy for the rise phase in each discharge. The average runaway energy ($\langle W_{\mathrm{RE}} \rangle$) was estimated as the mean of the product of the ith energy bin (W^{i}_{RE}) with binwidth of 100 keV and its corresponding recorded valid photon counts (n^{i}_{RE}), i.e.

$$\langle W_{\mathrm{RE}} \rangle = \frac{\sum_i W^i_{\mathrm{RE}} n^i_{\mathrm{RE}}}{\sum_i n^i_{\mathrm{RE}}}. \tag{1}$$

The valid photon counts from pulse height analysis, has been estimated in 100 keV binwidths, considering the fact that the detector set-up has an energy resolution of 80–100 keV. In order to build up statistics, this estimation has been made by considering a set of five identical discharges. The variations in the average energies between different repeatable discharges were found to vary mostly in the range of 100–200 keV.

A plot of the average runaway energy in the rise phase ($\langle W^{\mathrm{rs}}_{\mathrm{RE}} \rangle$) is shown in figure 6a. We do find that the average energy of the runaway electrons lost to the limiter is clustered within a range of 100–225 keV for $20.4 < E_{\mathrm{T}} < 45.9$ V/m. The corresponding number of photon bursts emitted during the rise phase are shown in figure 6b. The average runaway energies in the rise phase ($\langle W^{\mathrm{rs}}_{\mathrm{RE}} \rangle$) along with the corresponding valid photon counts (n_{RE}), for the E_{T} scan in the high-B_{T} range are shown in figure 7. The runaway energy $\langle W^{\mathrm{rs}}_{\mathrm{RE}} \rangle$ is seen to vary in the range 1.1–1.6 MeV (figure 7a).

Considering that LQ and NQ discharges of the SINP tokamak show characteristic differences in their evolution, as well as in the observed HX bursts [26], it must be noted here, that the two regimes of discharges can be demarcated on the basis of the edge safety factor attained at peak current (q^{pk}_a). It must be stated here that discharges, in the low-B_{T} scan, with $E_{\mathrm{T}} \geq 20.4$ V/m attains $q^{\mathrm{pk}}_a < 1.55$ (figure 8a).

In fact, for $q^{\mathrm{pk}}_a < 1.2$, which indicates regions wherein $E_{\mathrm{T}} > 35.7$ V/m, in the low-B_{T} regime, the current crash in the rise phase is sometimes so severe that the discharge is almost quenched ($I_{\mathrm{p}} \sim 0$–500 A), before the recovery takes place. Figure 8b shows that all discharges are with $q^{\mathrm{pk}}_a > 2$ in the high-B_{T} regime.

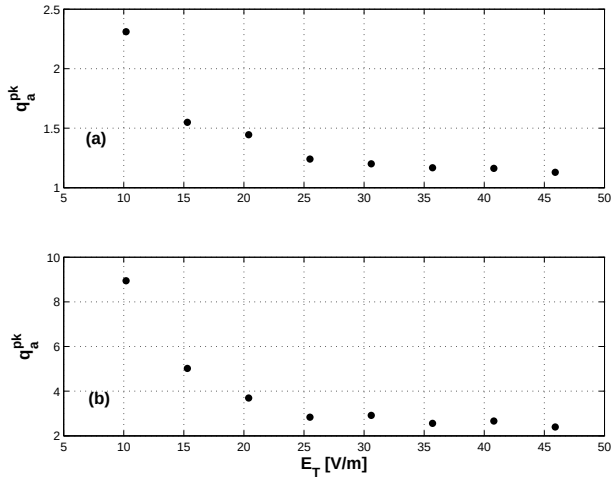

Figure 8. The variation q^{pk}_a with E_{T} scan in the (**a**) low-B_{T} regime and (**b**) high-B_{T} regime. Scatter in data over identical discharges is within the range of 0.5.

In order to correlate the edge safety factor at the peak current of a discharge ($q_a^{\rm pk}$) to the edge safety factor ($q_a^{\rm HXR}$), where the loss of hard X-ray bursts are observed, a plot of $q_a^{\rm pk}$ against $q_a^{\rm HXR}|_{\rm min}$ (the value of the edge safety factor, where the last hard X-ray burst is observed in the rise phase) is plotted for both high-$B_{\rm T}$ and low-$B_{\rm T}$ discharges (figure 9). Here a linear relation is observed for both sets of discharges. As this paper is concerned with comparison of the runaway dynamics in LQ and NQ discharges, the above-mentioned linear relation allowed us to correlate the runaway energies in the rise phase for different discharges ($\langle W_{\rm RE}^{\rm rs}\rangle$) with $q_a^{\rm pk}$.

Thus, to look at the transitional behaviour in the runaway performance with $q_a^{\rm pk}$, we have plotted $\langle W_{\rm RE}^{\rm rs}\rangle$ vs. $q_a^{\rm pk}$ (figure 10a). Figure 10a shows that this demarcation occurs at $q_a^{\rm pk} \approx 1.5$, indicating the possibility of the observance of a difference in behaviour being attributed to the effect of the NQ to LQ discharge transition on the runaway electrons itself. It must be stated here, that we were not able to obtain discharges in the range $1.55 < q_a^{\rm pk} < 2.3$. A change in $E_{\rm T}$ just saw a jump in the value of $q_a^{\rm pk}$ in the subsequent discharge.

A plot of $\langle W_{\rm RE}^{\rm rs}\rangle$ dependence on $q_a^{\rm pk}$ for the high-$B_{\rm T}$ discharges is shown in figure 10b. The plot shows that in the NQ discharges, $\langle W_{\rm RE}^{\rm rs}\rangle$ is in the range of ∼800–1650 keV. On the other hand, the LQ regime (figure 10a) shows the tendency for the runaway energies to be clustered around 100–200 keV. Further, one can note, that the LQ discharges, obtained in this scan, emitted $\langle W_{\rm RE}^{\rm rs}\rangle \sim 350$ keV at $q_a^{\rm pk} = 2.3$. It must be again stated that from figure 10a it is a bit difficult to obtain discharges with $q_a^{\rm pk}$ for $1.55 < q_a^{\rm pk} < 2.3$, which is the reason for the lack of data in the intermediate regime. It is also to be noted that the mismatch in the energies at about $2.3 < q_a^{\rm pk} < 2.34$ for the discharges at the two values of $B_{\rm T}$ can be attributed to a shift of the linear relation between $q_a^{\rm HXR}|_{\rm min}$ and $q_a^{\rm pk}$ at these sets of values, with ($q_a^{\rm pk}$, $q_a^{\rm HXR}|_{\rm min}$) being (2.34, 2.61) for the higher $B_{\rm T}$ discharge and (2.3, 3.4) for the lower $B_{\rm T}$ discharge. This implies that the hard X-ray bursts are observed to be lost much earlier in the rise phase of the lower $B_{\rm T}$ discharge when compared with the higher one. This could also be an effect of the higher value of $B_{\rm T}$ itself, which could be viewed as a better confinement of the runaway electrons, within the discharge. One can still state that the two different regions (LQ and NQ) of

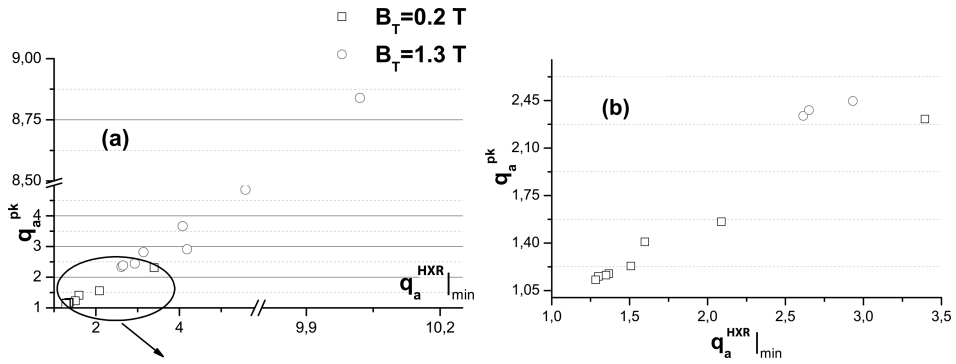

Figure 9. The variation $q_a^{\rm pk}$ with $q_a^{\rm HXR}|_{\rm min}$ for the low-$B_{\rm T}$ regime (open square) and high-$B_{\rm T}$ regime (open circle). Plot (**b**) is the expanded version of plot (**a**). Scatter in data over identical discharges is within the range of 0.5.

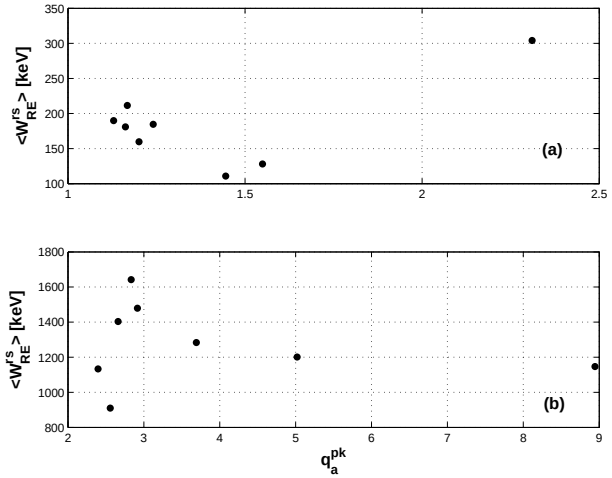

Figure 10. The variation of average runaway energy in the rise phase ($\langle W_{\rm RE}^{\rm rs}\rangle$) with edge safety factor at peak current ($q_a^{\rm pk}$) for both (**a**) low-$B_{\rm T}$ and (**b**) high-$B_{\rm T}$ discharge regimes during the variation of the applied $E_{\rm T}$. Scatter in data over identical discharges is within the range of 100 keV.

discharge evolution in the SINP tokamak are qualitatively reflected in their runaway behaviour too.

4. Estimations of diffusion and confinement time

The study of transport properties of the high-energy electrons can provide an insight into the differences of their behaviour in the different q_a regimes. Estimations of the diffusion coefficient of runaway electrons provide useful information about the mechanisms governing the anomalous particle transport in tokamaks.

4.1 *Measurements and estimates*

Measurement of high-energy electrons in the SINP tokamak is confined to the observance of limiter bremsstrahlung [37]. Hence, using the simple diffusion equation along with a source term (S_r) [38]

$$\frac{\delta n}{\delta t} = \frac{\delta}{\delta r}\left(D_{\rm RE}\frac{\delta n}{\delta r}\right) + S_r \tag{2}$$

the runaway diffusion coefficient $D_{\rm RE}$ is calculated, from the mean plasma column velocity ($\langle v_{\rm p}\rangle$) during the observation of HX bursts ($\Delta t_{\rm HX}^{\rm dur}$). The source term in this case can be represented as $S_r = \frac{n}{\tau_a} - \frac{n}{\tau_{\rm c}}$ where τ_a and $\tau_{\rm c}$ are the acceleration time due to the electric field and collision times respectively. If a transformation of the type, $n_1 = n\exp(-t/\tau_{\rm eff})$ is considered, the above diffusion equation reduces

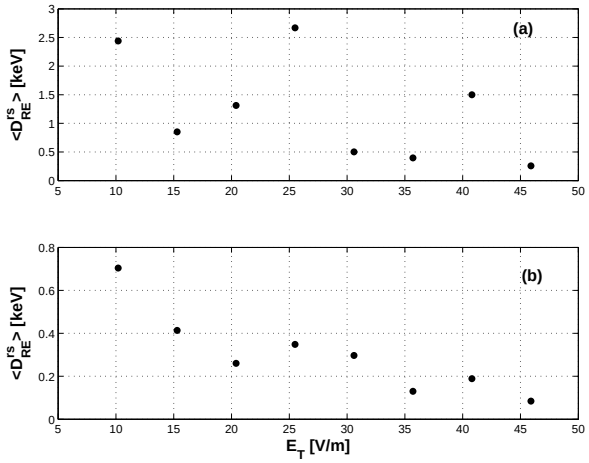

Figure 11. The variation of runaway diffusion coefficient in the rise phase ($\langle D_{\rm RE}^{\rm rs}\rangle$) with $E_{\rm T}$ for (**a**) low-$B_{\rm T}$ and (**b**) high-$B_{\rm T}$ discharge regimes. Scatter in data in the low-$B_{\rm T}$ discharge regimes is as large as 5 $\rm m^2/s$ whereas that in the high-$B_{\rm T}$ discharges are in the range 0.05–0.1 $\rm m^2/s$.

to a source-free equation in n_1. Here, $\frac{1}{\tau_{\rm eff}} = \frac{1}{\tau_a} - \frac{1}{\tau_{\rm c}}$. Under these considerations, the method followed in ref. [38] can be utilized for estimating the runaway diffusion coefficient, provided $t \ll \tau_{\rm RE}$. $\tau_{\rm RE}$ is the runaway confinement time. The hard X-ray bursts begin to be observed around 150–350 μs (figure 3). So we can assume $\tau_{\rm RE} \sim \tau_a \approx$ 100–300 μs. In fact, $E_{\rm T}$ values are also quite high in the rise phase (from 10 V/m to as high as 40 V/m), which implies that one can neglect $\tau_{\rm c}$ for the present set of discharges also. However, incorporating $\tau_{\rm c}$ reduces the effect of the source term. Thus, for the discharges presented in this paper, $D_{\rm RE}$ can be calculated by solving eq. (2), to obtain [38]

$$D_{\rm RE} = \left(\frac{2\langle v_{\rm p}\rangle}{(1-\tilde{F}_{\rm RE})}\right)^2 \frac{\Delta t_{\rm HX}^{\rm dur}}{\pi}, \tag{3}$$

where $\tilde{F}_{\rm RE} = \langle W_{\rm RE}\rangle / W_{\rm RE}^{\rm max}$ is the normalized hard X-ray flux, $\langle W_{\rm RE}\rangle$ is the average runaway energy and $W_{\rm RE}^{\rm max}$ is the maximum runaway energy emitted during the burst period of $\Delta t_{\rm HX}^{\rm dur}$. This relation is used to make a rough calculation of $D_{\rm RE}$ in the rise phase ($D_{\rm RE}^{\rm rs}$) using an average column shift velocity during the period of observance of the limiter bremsstrahlung.

Therefore, an estimation of the diffusion coefficient in the low- and high-$B_{\rm T}$ discharges, during the HX bursts in the rise phases of $E_{\rm T}$ scan, are represented in figure 11. It must be stated here, that the value of $\langle v_{\rm p}\rangle$ depends on the discharge evolution itself, over which there is no control due to the absence of a feedback control in the SINP tokamak. As the value of $D_{\rm RE}$ is dependent on $\langle v_{\rm p}\rangle$, a more careful analysis of the diffusion coefficient is not possible here. It must, however, be stated that the order of the average value of $D_{\rm RE}^{\rm rs}$ is different in the two scans, with 0.3 $\rm m^2/s < \langle D_{RE}^{rs}\rangle <$ 3 $\rm m^2/s$ in the low-$B_{\rm T}$ scan. In some cases, it is even observed to be as large as 10 $\rm m^2/s$. In the high-$B_{\rm T}$ scan, however, it is observed

to be in the range of $0.1 < \langle D_{\rm RE}^{\rm rs} \rangle < 1$ m^2/s with a scatter of 0.05–0.1 m^2/s. This larger scatter of data in LQ discharges is more likely to be the result of the lower statistical photon counts. This implies that the discharges with $q_a^{\rm pk} < 2$, has $D_{\rm RE}^{\rm rs}$ in the range of 0.3–10 m^2/s whereas in the discharges of $q_a^{\rm pk} > 2$, $D_{\rm RE}^{\rm rs}$ is estimated to be in the range of 0.1–1 m^2/s. Thus, we can conclude that the runaways experience enhanced transport in the LQ discharges in comparison to the NQ discharges.

The corresponding runaway confinement time ($\tau_{\rm RE}$) can be estimated using the relation [39]

$$D_{\rm RE} = \frac{a^2}{5.6\tau_{\rm RE}}. \tag{4}$$

One can then have $\tau_{\rm RE}$ in the range of 200–1000 μs in the LQ regime and 1–20 ms in the NQ regime, if one considers that the runaways are generated at the minor axis of the torus. One should, however, ideally consider a location towards the edge, where runaways can be assumed to be generated. This consideration can be safely assumed, if the probable location of runaway generation ($a_{\rm RE}$) is evaluated, using the relation [1,40]

$$a_{\rm RE} = a_l \left[1 - \frac{\sqrt{\gamma_{\rm RE}^2 - 1}}{(2R_0/a_l)\,(I_{\rm p}/I_{\rm A})} \right]. \tag{5}$$

Here, $\gamma_{\rm RE}$ is the relativistic gamma factor of the runaway energy beam observed by the detector, $I_{\rm A} = 17$ kA is the Alfven current, R_0 is the major radius and a_l is the radius at which the electron strikes a target. In the experiments presented in this paper, $a_l = 0.075$ m is the limiter radius. Using experimental values of $\langle W_{\rm RE}^{\rm rs} \rangle = 150$ keV and $\langle W_{\rm RE}^{\rm rs} \rangle = 400$ keV for LQ discharges with plasma currents $I_{\rm p} = 10$–20 kA and $\langle W_{\rm RE}^{\rm rs} \rangle = 1000$ keV and $\langle W_{\rm RE}^{\rm rs} \rangle = 1300$ keV for NQ discharges with plasma current $I_{\rm p} = 20$–40 kA, $a_{\rm RE}$ is evaluated to be in the range of 0.055–0.07 m. Further, discharges within the SINP tokamak [28,29] are observed to have a sustained hollow profile even after the initial current penetration phase, with the peaking to be around $r/a = 0.85$. Hence for an estimate, the radius of generation of runaway electrons is assumed to be about $a_{\rm RE} = 0.065$ m, considering that $a_l = 0.075$ m in this paper. This means that we must consider $a = 0.01$ m in eq. (4). This yields $\tau_{\rm RE}$ in the range of 3.5–17 μs in the LQ regime and 17–357 μs in the NQ regime. This estimation looks more realistic considering the discharge duration (∼a few ms) as well as the time within which one observes the initial limiter bremsstrahlung bursts in the rise phase to be ∼ tens of μs. Thus, enhanced confinement of runaway electrons is observed in the NQ discharges.

4.2 *Estimates of magnetic fluctuation*

The transport characteristics of the high-energy electrons in the SINP tokamak is considered from the point of view of turbulent transport. It is believed that with runaways remaining ideally collisionless within the discharge, its transport in the plasma core arises primarily from the magnetic fluctuations. Hence, we consider the runaway transport to be dominated by magnetic turbulence. Myra and Catto

[41] deduced an expression that related the runaway diffusion coefficient with the magnetic coefficient and in turn with the electron thermal conductivity. From a more general scenario, where the effect of electrostatic turbulence also is considered, an expression of the runaway diffusion coefficient is given as [18]

$$D_{\mathrm{RE}} = \pi q R\left[\beta_{\mathrm{RE}} c\left(\frac{\langle b\rangle}{B_{\mathrm{T}}}\right)^2 + \frac{1}{\beta_{\mathrm{RE}} c}\left(\frac{\langle E\rangle}{B_{\mathrm{T}}}\right)^2 + 2\frac{\langle b\rangle\langle E\rangle}{B_{\mathrm{T}}^2}\cos\delta\right], \tag{6}$$

where $\langle b\rangle$ and $\langle E\rangle$ are the magnetic and electric fluctuating fields and δ is the phase of $\langle E\rangle$ with $\langle b\rangle$. The magnetic fluctuation levels in the SINP tokamak are found to be $\langle b\rangle/B_{\mathrm{T}} \sim 10^{-2}$–$10^{-4}$ and the electrostatic fluctuation levels are found to be of the order of $\langle E\rangle/B_{\mathrm{T}} \sim 10^3$–$10^4$ m/s with the larger levels of fluctuations being observed in the LQ discharges. But, the fact that the contributions from the magnetic fluctuations is proportional and that of the electrostatic fluctuations inversely proportional to the velocity of light, implies that the contribution from the magnetic fluctuations $[\beta c(\langle b\rangle/B_{\mathrm{T}})^2 \sim (30000-3)\beta]$ is dominant when compared with the electrostatic fluctuations $[\frac{1}{\beta c}(\langle E\rangle/B_{\mathrm{T}})^2 < (0.01-1)/3\beta]$ in the SINP tokamak. The cross term will be in the range $(0.2$–$200)\cos\delta$. At the worst possible scenario of low magnetic fluctuations and high electrostatic fluctuations, for very low energies ($W_{\mathrm{RE}} = 150$ keV), the dominant contribution will still come from the magnetic fluctuation term in the discharges presented in this paper. Hence, we have considered only the effect of the magnetic fluctuations on runaway electrons in the rest of this paper.

The contribution of the magnetic turbulence alone is given as

$$D_{\mathrm{RE}} = \Upsilon D_{\mathrm{M}} v_{||}, \tag{7}$$

$$= \Upsilon q R(\langle b\rangle/B_{\mathrm{T}})^2 v_{||}, \tag{8}$$

$$\approx \chi v_{\mathrm{RE}}/v_{\mathrm{the}}, \tag{9}$$

where D_{M} is the magnetic diffusion coefficient, v_{the} and v_{RE} are the respective thermal and runaway component velocities. Υ is a correction factor due to drift orbit averaging and is mainly dependent on the ratio of the drift-orbit displacement d_r to the radial mode width, σ. Mathematically, it can be written as [42]

$$\Upsilon = 1, \quad \text{if} \quad d_r < \sigma$$

$$= \frac{\Upsilon_0}{\sqrt{\gamma_{\mathrm{RE}}^2 - 1}}\frac{2\cos\theta}{1+\cos\theta} \quad \text{otherwise}, \tag{10}$$

where $\Upsilon_0 \sim \sigma e B_{\mathrm{T}}/m_e q_0 c$, where $\cos\theta$ is as indicated in ref. [42], with θ being the pitch angle. $\sigma \approx 1/m$, where m is the poloidal mode number roughly given by a/ρ_i (where ρ_i is the ion Larmor radius). d_r is given as [21]

$$d_r = \frac{m_e q_0 \gamma_{\mathrm{RE}}}{e B_{\mathrm{T}} \beta_{\mathrm{RE}} c}\left(\beta_{\mathrm{RE}}^2 c^2 + \frac{v_\perp^2}{2}\right), \tag{11}$$

where β_{RE} and γ_{RE} are the relativistic beta and gamma factors of the runaway beams respectively; $v_{||} = \beta_{\mathrm{RE}} c$ and $v_\perp$ are the parallel and perpendicular (with

Table 1. Estimated values of the drift orbit displacement (d_r) and the magnetic fluctuation ($\langle b\rangle/B_{\rm T}$) for a set of edge safety factor (q_a), runaway energy ($W_{\rm RE}$) and runaway diffusion coefficient ($D_{\rm RE}$).

q_a	$W_{\rm RE}$ (keV)	$D_{\rm RE}$ (m^2/s)	d_r (mm)	$\langle b\rangle/B_{\rm T}$
		Low-$B_{\rm T}$ scan		
1.15	200	0.2	9.625	5.250×10^{-5}
1.5	100	1	8.502	1.157×10^{-4}
2.3	300	2.5	24.55	1.243×10^{-4}
		High-$B_{\rm T}$ scan		
2.4	1100	0.07	9.587	1.875×10^{-5}
2.8	1600	0.35	15	3.922×10^{-5}
3.75	1300	0.25	17.047	3.684×10^{-5}
5	1200	0.4	21.354	1.054×10^{-4}
9	1100	0.7	35.95	3.712×10^{-5}

respect to the toroidal magnetic field $B_{\rm T}$) electron velocities respectively; c is the velocity of light and q_0 is the average safety factor over the drift orbit displacement. Taking a typical value for average energy as 100 keV at $B_{\rm T} = 0.2$ T and $q_{\rm a} \sim 1.5$, as observed in the SINP tokamak (figure 6), we would have assumed a temperature of $\sim$10 eV, $d_r \approx 0.0085$ m (table 1). This means $d_r < \sigma$, and for all practical purposes one can consider $\Upsilon \sim 1$ from eq. (10). Thus, if the runaway transport is the result of the magnetic fluctuations within the discharge, one will obtain ($\langle b\rangle/B_{\rm T} \sim 10^{-4}$) in the LQ regime. In fact, using eqs (8), (10) and (11), the estimated values of the drift orbit displacement (d_r) and the magnetic fluctuation levels ($\langle b\rangle/B_{\rm T}$), for some of the low-$B_{\rm T}$ and high-$B_{\rm T}$ scan discharges, are given in table 1. The calculations were made, assuming the plasma temperature to be $\sim$10 eV.

In order to confirm whether the runaway transport is a result of the magnetic turbulence within the system for the SINP tokamak, we measured $\langle b\rangle/B_{\rm T}$ from a magnetic signal. The magnetic signal used for this purpose was from a poloidal magnetic coil, filtered in the range of 1–200 kHz and the results are presented in figure 12. The fluctuations are in the range $\sim 10^{-4}$–10^{-5} in NQ and in the range $\sim 10^{-2}$–10^{-4} in the LQ regime. In fact, the discharges show that as we go from NQ to LQ discharges, the magnetic fluctuation levels not only increase, but also scatter from discharge to discharge, for a given plasma condition. Further, the estimate of figure 12 are from a poloidal field coil, whereas $\langle b\rangle$ can ideally be estimated from a radial field coil, which was not present during these experiments. This can explain the mismatch of order in the estimates of table 1 and figure 12. However, keeping this fact in mind, it does indicate that the trend of estimates from the magnetic coil signals for transition from NQ to LQ discharges seem to match with that of the estimates of the limiter bremsstrahlung observations.

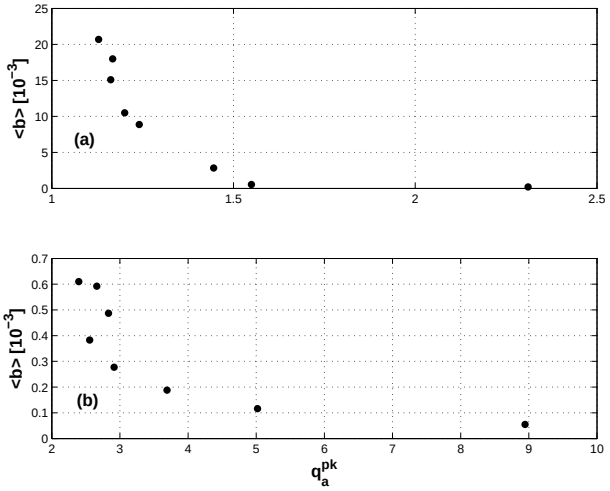

Figure 12. The estimation of the magnetic fluctuations ($\langle b\rangle/B_{\rm T}$) with $q_a^{\rm pk}$ evaluated from the poloidal magnetic coil signal on the outer side of the torus, in the rise phase of (**a**) low-q_a scan, (**b**) normal q_a scan. Scatter in data in the low-$B_{\rm T}$ discharge regimes is within the range of 10×10^{-3} whereas that in the high-$B_{\rm T}$ discharges is in the range 0.5×10^{-3}.

5. Conclusions and discussions

In this scan, we have seen a distinct difference in the runaway behaviour in the NQ and LQ discharges. Some of the features noticed in the scans can be categorized as follows:

- Higher current discharges are observed to confine higher energetic runaways.
- Runaway confinement properties in the LQ discharges are observed to degrade when compared with NQ discharges.
- The runaway diffusion coefficients ($D_{\rm RE}$) are observed to be $\sim$0.1–1 m^2/s in the NQ regimes with the average runaway energies 900 keV $< \langle W_{\rm RE}^{\rm rs}\rangle <$ 1600 keV whereas in the LQ regime, we have runaway diffusion coefficient in the range of $0.3 < D_{\rm RE} < 10$ m^2/s for average runaway energies ($\langle W_{\rm RE}^{\rm rs}\rangle$) less than 300 keV.
- The magnetic fluctuation levels are also observed to be higher in the LQ discharges ($\sim 10^{-2}$–10^{-4}) when compared with the NQ ($\sim 10^{-4}$–10^{-5}) regimes.

The parametric scan has shown that the runaway dynamics have distinctly different features in the LQ and NQ regimes due to the differences in the current profiles in the two regimes. It was observed [32] that the LQ discharges in the SINP tokamak had a sustained hollow profile in comparison to a more peaked profile in the NQ regime, after the initial current penetration. Hence, it possible that in NQ discharges runaway electrons are generated in orbits closer to the minor axis when compared with the LQ discharges. This should explain the better confinement of runaways in NQ discharges.

Acknowledgements

The authors wish to acknowledge members of the Plasma Physics Division as well as Workshop Section of Saha Institute of Nuclear Physics for their help towards performing the experiments.

References

[1] H Knoepfel and D A Spong, *Nucl. Fusion* **19**, 785 (1979)
[2] R D Gill *et al*, *Nucl. Fusion* **40**, 163 (2000)
[3] R Yoshino *et al*, *Nucl. Fusion* **39**, 151 (1999)
[4] T Fülöp, H M Smith and G Pokol, *Phys. Plasmas* **16**, 022502 (2009)
[5] M Bakhthiari *et al*, *Phys. Rev. Lett.* **94**, 215003 (2005)
[6] M Bakhtiari, H Tamai, Y Kawano, G J Kramer, A Isayama, T Nakano, Y Kamiyal, R Yoshino, Y Miura, Y Kusama and Y Nishida, *Nucl. Fusion* **45**, 318 (2005)
[7] J R Martn-Solis, B Esposito, R Snchez and G Granucci, *Nucl. Fusion* **44**, 974 (2004)
[8] Yu K Kuznetsov, R M O Galvão, V BellintaniJr, A A Ferreira, A M M Fonseca, I C Nascimento, L F Ruchko, E A O Saettone, V S Tsypin and O C Usuriaga, *Nucl. Fusion* **44**, 631 (2004)
[9] V Riccardo and JET EFDA contributors, *Plasma Phys. Control. Fusion* **45**, A269 (2003)
[10] P Helander, L-G Eriksson and F Andersson, *Plasma Phys. Control. Fusion* **44**, B247 (2002)
[11] D G Whyte, T C Jernigan, D A Humphreys, A W Hyatt, C J Lasnier, P B Parks, T E Evans, M N Rosenbluth, P L Taylor, A G Kellman, D S Gray, E M Hollmann and S K Combs, *Phys. Rev. Lett.* **89**, 055001 (2002)
[12] J D Strachan, *Nucl. Fusion* **16**, 743 (1976)
[13] A D Cheetam, J A How, G R Hogg, H Kuwahara and A H Morton, *Nucl. Fusion* **23**, 1694 (1983)
[14] V V Plyusnin, J A C Cabral, H Figueiredo and C A F Varandas, *28th EPS Conference on Contr. Fusion and Plasma Phys.*, Funchal, 18–22 June 2001, **ECA–25A**, 601 and http://www.cfn.ist.utl.pt/EPS2001/fin/pdf/P2.031.pdf
[15] C W Barnes and J D Strachan, *Nucl. Fusion* **22**, 1090 (1982)
[16] C W Barnes and J D Strachan, *Phys. Fluids* **26**, 2668 (1983)
[17] O J Kwon, P H Diamond, F Wagner, G Fussmann, ASDEX and NI Teams, *Nucl. Fusion* **28**, 1931 (1988)
[18] B Esposito, R Martin Solis, P van Belle, O N Jarvis, F B Marcus, G Sadler, R Sanchez, B Fischer, P Froissard, J M Adams, E Cecil and N Watkins, *Plasma Phys. Control. Fusion* **38**, 2035 (1996)
[19] I Enthrop, *Confinement of relativistic runaway electrons in tokamak plasmas*, Thesis work submitted in December 1999 at Technische Universiteit Eindhoven; http://alexandria.tue.nl/extra2/9903850.pdf
[20] Y Peysson and F Imbeaux, *Rev. Sci. Instrum.* **70**, 3987 (1999)
[21] B Esposito, J R Martin-Solis, F M Poli, J A Mier, R Sanchez and L Panaccione, *Phys. Plasmas* **10**, 2350 (2003)
[22] V Antoni, *Plasma Phys. Control. Fusion* **39**, B223 (1997)
[23] J C Ingraham, R F Ellis, J N Downing, C P Munson, P G Weber and G A Wurden, *Phys. Fluids* **B2**, 143 (1990)

[24] Y Yagi, Y Hirano, T Shimada and Y Maejima, *Jpn J. Appl. Phys.* **35**, 4064 (1996)
[25] Y Yagi, V Antoni, M Bagatin, D Desideri, E Martines, G Serianni and F Vallone, *Plasma Phys. Control. Fusion* **39**, 1915 (1997)
[26] A N S Iyengar, R Pal, S Lahiri and S Mukhopadhyay, *Nucl. Fusion* **38**, 1117 (1998)
[27] S Lahiri, A N Sekar Iyengar, S Mukhopadhyay and R Pal, *Nucl. Fusion* **36**, 254 (1996)
[28] S Lahiri, A N Sekar Iyengar, S Mukhopadhyay and R Pal, *Pramana – J. Phys.* **56**, 615 (2001)
[29] S Lahiri, A N Sekar Iyengar, S Mukhopadhyay and R Pal, *Pramana – J. Phys.* **58**, 79 (2002)
[30] Z Yoshida, Y Murakami, H Morimoto, J Matsui, D Nagahara, S Takeji and N Inoue, *Nucl. Fusion* **30**, 762 (1990)
[31] P K Chattopadhyay, *Studies of anomalous ion heating in very low q_a discharges of the SINP-tokamak*, Thesis work submitted in Aug. 1996 (Jadavpur University, Calcutta, West Bengal, India)
[32] Sudeshna Lahiri, *Investigations of low q_a discharges in the SINP Tokamak*, Thesis work submitted in March 1999 (University of Jadavpur)
[33] Y Murakami, Z Yoshida and N Inoue, *Nucl. Fusion* **28**, 449 (1988)
[34] Y Murakami, *Study on MHD isntability for equilibria with monotonic and non-monotonic q-profiles*, Thesis work submitted in 1988 (University of Tokyo, Japan, 1988)
[35] K Suzuki, Z Yoshida, K Kusano, *Nucl. Fusion* **31**, 179 (1991)
[36] Z Yoshida, N Inoue, T Fujita, H Morimoto, J Matsui, S Takeji, D Nagahara, J Okabe, H Nihei and J Morikawa, *Nucl. Fusion* **31**, 532 (1991)
[37] Ramesh Narayanan, A N Sekar Iyengar and R Pal, *Pramana – J. Phys.* **55(5&6)**, 719 (2000)
[38] P J Catto, J Y Myra, P W Wang, A J Wootton and R D Bengtson, *Phys. Fluids* **B3**, 2038 (1991)
[39] I Entrop, N J Lopes Cardozo, R Jaspers and K H Finken, *Plasma Phys. Control. Fusion* **40**, 1513 (1998)
[40] A J Russo and R B Campbell, *Nucl. Fusion* **33**, 1305 (1993)
[41] J Y Myra and P J Catto, *Phys. Fluids* **B4**, 176 (1992)
[42] J R Martin-Solis, R Sanchez and B Esposito, *Phys. Plasmas* **6**, 3925 (1999)